Polymer Testing 95 (2021) 107133

Contents lists available at ScienceDirect

Polymer Testing

journal homepage: http://www.elsevier.com/locate/polytest

Effect of compatibilizers on lignin/bio-polyamide blend carbon precursor filament properties and their potential for thermostabilisation and carbonisation

R. Muthuraj, M. Hajee, A.R. Horrocks, B.K. Kandola *

Institute for Materials Research and Innovation (IMRI), University of Bolton, Deane Road, Bolton, BL3 5AB, UK

ARTICLE INFO

Keywords:
Compatibilizer
Lignin
Polyamide
Blends
Filaments
Precursor
Thermal stabilization
Carbonization

ABSTRACT

Biobased blends from hydroxypropyl modified lignin (TcC) and a biobased polyamide (PA1010) were produced by continuous sub-pilot scale melt spinning process. A reactive compatibilization was employed with the help of two different compatibilizers (ethylene-acrylic ester-maleic anhydride (MA) and ethylene-methyl acrylate-glycidyl methacrylate (GMA)) to enhance the compatibility between the TcC and PA1010. The enhanced compatibility between the TcC and PA1010 achieved by reaction between hydroxyl groups with maleic anhydride groups in the MA compatibilizer or epoxy groups in the GMA compatibilizer via nucleophilic substitution, was confirmed by chemical (Fourier infrared measurements), physical (glass transition, melting and crystallization behaviour), rheological, morphological and tensile properties of the filaments from compatibilized blends. MA compatibilizer required a higher concentration (2 phr) than GMA (1 phr) to achieve an optimal performance because of the difference in the reactive group's concentration within the each compatibilizer. The MA compatibilizer though was more effective than GMA. The precursor blended filaments were successfully carbonized in a lab scale experiment to yield coherent carbon fibres with tensile stress values of 192 ± 77 and 159 ± 95 MPa; and moduli of 16.2 and 13.9 GPa respectively for uncompatibilised and 2% MA compatibilized blends. That the compatibilized carbon fibre properties are slightly inferior may be attributed to the need to accurately control and optimise applied stress during the thermostabilisation and carbonization stages. Notwithstanding, these differences, the results indicate the potential benefit of using compatibilized TcC/PA1010 blend filaments as carbon fibre precursors.

1. Introduction

While interest in biopolymers continues to increase as replacements for petroleum-based polymers, their increased production remains challenging not least because of increased cost but also their inferior properties [1]. However, one solution is the development of biopolymer blends in which a main focus lies in maximising their miscibility/compatibility often by the addition of compatibilizers [2]. Lignin is the second most abundant biopolymer in the world and as a by-product from the paper and pulp industry results in about 70 million tonnes produced globally each year. Unfortunately at the present time, only 5% is effectively used towards producing useful chemicals due to its complex molecular structure, with the remainder being burnt to produce energy [3,4]. The base phenylpropane groups in lignin consist of syringyl, guaiacyl and p-hydroxy phenol units covalently bonded to form a complex matrix to which several functional groups, such as carbonyl, methoxyl and hydroxyl are attached and which allow lignin macromolecules to have a high polarity. These characteristics, suggest that lignin is a promising material as a component within multicomponent polymeric blends [5]. Due to its heterogeneous, aromatic structure the simple addition of a second polymer, unless highly compatible, creates a heterogeneous structure which often makes the blend too brittle for most targeted applications [5]. Therefore, lignin requires degree of chemical modification to allow it to develop acceptable properties [6], which would improve its usefulness at the expense of increased cost. However, lignin has a high carbon content (≥60%), which makes it an ideal candidate to produce carbon fibre precursors and while both hardwood and softwood lignin fibres have been produced using the melt spinning process, it has been reported that spooled lignin fibres are difficult to wind without the lignin being pre-treated or

* Corresponding author.
E-mail address: b.kandola@bolton.ac.uk (B.K. Kandola).

https://doi.org/10.1016/j.polymertesting.2021.107133
Received 31 December 2020; Received in revised form 8 February 2021; Accepted 15 February 2021
Available online 22 February 2021

modified [7].

Polymer blending offers a means of potentially solving this problem and so improve mechanical performance, morphology, rheology and other lignin-deficient properties [8]. Reported examples include miscible lignin blends with poly(lactic acid), poly(ethylene terephthalate) and polyamides, which identify important factors such as lignin pre-treatment to enhance overall dispersion and achieve improved processability and melt spinnability [9,10]. Recent work by ourselves has shown that selected modified lignins may be blended with a number of biopolyamides such as PA11, PA1010 and PA1012 to yield blends of varying degrees of heterogeneity depending on the lignin type, the polyamide structure and blend composition [9,10]. This work has also shown that the addition of a biopolyamide increases yield for char formation when heated under an inert atmosphere like nitrogen. This feature would increase the suitability of a melt processable lignin blend precursor for bio-based carbon fibre production [11].

However, a key to achieving this goal is the maximisation of blend compatibility and our previous work has demonstrated that while maximum lignin contents in lignin/PA as high as 50 wt% give rise to melt extrudable precursor filaments having both acceptable mechanical and char-forming properties, their poor homogeneity still remains an issue [9,10]. Furthermore, the need to be able to convert the derived thermoplastic precursor fibres to a cross-linked, thermoset structure through a stabilization process [9], will be increased in efficiency with increased blend homogeneity. Hence the use of compatibilizers offers an obvious means of achieving this aim [12]. The interactions between lignin and a polymer such as a polyamide arise from weak van der Waal's forces and hydrogen bonds [5]. Compatibilization adds to these inherent intermolecular forces by reducing the interfacial tension between component surfaces, thus increasing the interfacial adhesion and greater dispersion of component domains thereby improving the homogeneity of the blend [13]. Other studies have reported that with the addition of reactive compatibilizers, the domain size of lignin, even at higher wt.% levels, is reduced [14,15]. Maleic anhydride is a well-known compatibilizer for polymer blends and it has been reported that it works both as a plasticizer and compatibilizer [16]. Generally, while biopolymers contain various functional groups favourable for interactions with compatibilizers, their effects in terms of morphological and structural modifications should be balanced against accompanying changes in properties for the specific applications [17–19]. Of especial interest to this current work are the improvements in polymer blend mechanical and morphological properties achieved by introducing suitable compatibilizers and their effect on the subsequent thermostabilisation and carbonization processes during the carbon fibre production.

In our earlier study, it was found that the hydroxypropyl modified hardwood lignin (TcC) is compatible with bio-based polyamides, but the performances of the laboratory-scale processed blends were not sufficient to enable prospective applications as carbon fibre precursor filaments to be achieved [9]. This study aims to explore whether the introduction of selected compatibilizers based on maleic anhydride or glycidyl methacrylate derivatives [1,13,16,20–23] could enable the more facile production of melt spun filaments from TcC and a bio-polymer polyamide (PA1010) using a laboratory-scale melt spinning system. Optimal concentrations of these compatibilizers introduced during the compounding stage, were determined based on the analysis of derived melt spun, TcC/PA1010 blend filaments physical properties, their thermostabilisation and carbonization behaviours and resulting carbon fibre tensile and morphological properties.

2. Materials and methods

The chemical structures of the selected materials are shown in Scheme 1. Hydroxypropyl modified organosolv lignin (TcC) with weight average molecular weight of 11357 g/mol and bio-based polyamide (PA1010, Vestamid® Terra DS) were procured from Tecnaro, Ilsfeld, Germany and Evonik Industries, Germany, respectively. The TcC modification methods are commercially restricted by the manufacturer but a detailed characterization of TcC can be found elsewhere [24]. Two random terpolymers including ethylene-acrylic ester-maleic anhydride (LOTADER® 4700) [MA] and ethylene-methyl acrylate-glycidyl methacrylate (LOTADER® AX8900)] [GMA] were sourced as compatibilizers from Arkema, France. The MA terpolymer consists of 1.3 wt% maleic anhydride groups while 8 wt% glycidyl methacrylate groups are present in GMA terpolymer. These terpolymers have a melt flow index of 7g/10 min for MA and 6g/10 min for GMA.

2.1. Melt compounding and melt-spinning extrusion of continuous filaments

The TcC lignin and PA1010 were dried overnight at 80 °C in an oven prior to compounding. Post-drying it was observed that the lignin still

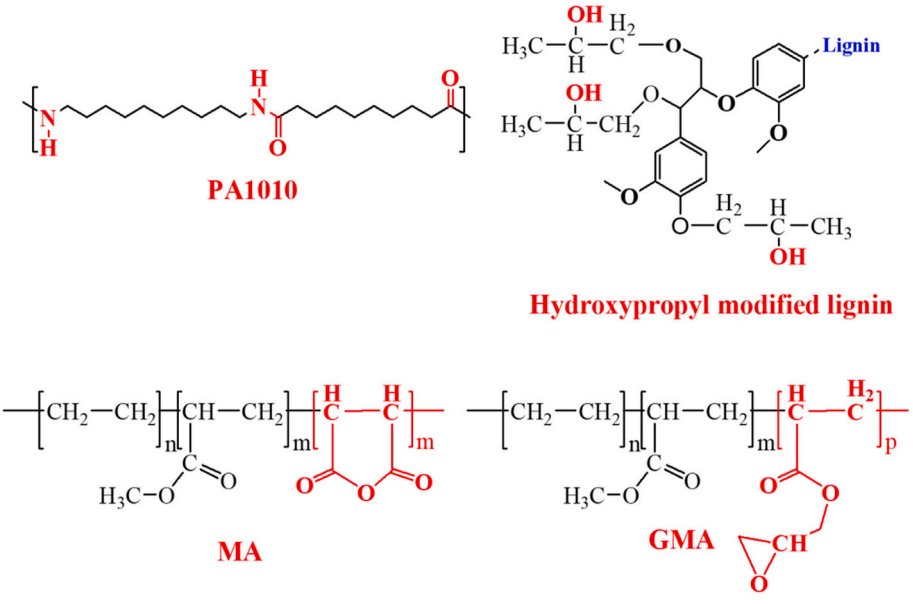

Scheme 1. Chemical structures of PA1010, hydroxylpropyl modified lignin, MA terpolymer and GMA terpolymer.

contained residual moisture of approximately 3%. An appropriate mixture was manually prepared in a plastic container by shaking the required amounts of TcC, PA1010, MA and GMA together prior to being fed into the twin-screw compounding extruder (Prism Eurolab 16, Thermo Fisher Scientific). The formulations provided in Table 1 were compounded using a screw speed of 100 rpm and a temperature profile between 180 and 190 °C over the six heating zones. The extrudates were passed through a water bath before being pelletized.

The filaments were produced from multi-kilogram of compounded pellets using a pilot-scale fibre extrusion technology (FET-101, UK) melt spinning system. The melt spinner consisted of five zones (feed zone, barrel zones, metering zone, die zone and pack zone) with an electrically driven screw, which had an internal diameter of 25 mm and an L/D ratio 30:1. The melt compounded TcC/PA1010 blends were introduced into the feed zone, transferred by the screw along the barrel zones at temperatures ranging from 185 to 195 °C with a screw speed of 25 rpm into the metering zone, which also enhanced mixing at 215 °C. Molten multifilament exited the die zone with a temperature of 220 °C via a filtration pack and a 24-hole spinneret (Φ = 0.8 mm) at a pressure of approx. 100–105 bar. The resulting filaments were cooled by air quenching (20 °C) and collected over a set of 3 rollers with roller speeds varying between 13 and 83 m/min and at a temperature of 60 °C before being wound on to cardboard tubes as shown in Fig. 1. Successful production of hundreds of meters of 24-count continuous tow of TcC/PA1010 blend filaments with a diameter of 102–127 μm.

2.2. Characterization of the compounded pellets

Oven dried (overnight at 80 °C) pellets were used to measure the rheological properties in the Discovery HR 1 Hybrid Rheometer (TA instruments, UK) at 200 °C using parallel plate geometry. The diameter of the parallel plate was 25 mm and the sample loading gap was 1 mm. The frequency sweep test was performed from 628 to 0.01 rad/s. A Thermo Scientific Nicolet 6700 Fourier Transform Infrared (FTIR) spectrometer was used to analyse the lignin, polyamide and compatibilizer blends as pellets at ambient temperature. The spectra were recorded from 4000 to 550 cm^{-1} with 32 scans and 4 cm^{-1} resolution. Glass transition temperatures (T_g) of samples were determined by dynamic mechanical analysis, DMA, (TA instruments Q800 DMA). In order to measure T_g values, about 2 g samples (lignin powder, PA1010 pellets, and PA1010/lignin blend pellets) were sandwiched between 0.6 mm thick aluminium sheets and wrapped in 0.05 mm thin aluminium foil to avoid particles/pellets loss during analysis [9]. The samples were heated at 3 °C/min from 25 to 200 °C with a 15 μm oscillating amplitude and 1Hz vibrating frequency in a dual cantilever mode.

Melting and crystallization behaviour of the blend pellets were analysed by differential scanning calorimetry, DSC, (TA Q2000 DSC, TA instruments, UK) under a nitrogen atmosphere (50 mL/min) with defined heat/cool/heat cycles. During the first cycle (heating), the temperature was increased from 0 to 200 °C at a heating rate of 10 °C/min and the subsequent first cooling cycle, returned the sample to 0 °C at a cooling rate of 5 °C/min. The second heating cycle heated the sample again from 0 to 200 °C at a heating rate of 10 °C/min. The initial heating cycle was used to remove the thermal histories of the samples. The cooling and re-heating cycles were considered for the analysis. The percentage crystallinity (x) of neat PA1010 was calculated as follows

$$x = \frac{\Delta H_m}{\Delta H_m^\circ} * 100$$

The percentage crystallinity (x) of PA1010 in TcC/PA1010 blends with and without MA and GMA was calculated as follows

$$x = \frac{\Delta H_m}{\Delta H_m^\circ\ (1 - \text{wt.\%})} * 100$$

Where ΔH_m is the melting enthalpy and ΔH_m° is the theoretical melting enthalpy of 100% crystalline PA1010 *i.e.,* 244 J/g [25]. Also, the weight fraction wt.% is the fraction of TcC lignin within the TcC/PA1010 blends.

Sample thermal stabilities were analysed using a TGA model SDQ-Q600 thermogravimetric analyser. Both thermogravimetric (TGA) and differential thermogravimetric (DTG) were recorded for around 10 mg samples under a nitrogen atmosphere of 100 mL/min and an increase in temperature from ambient to 900 °C at a heating rate of 20 °C/min.

2.3. Characterisation of the spun filaments for mechanical and morphological properties

Prior to measuring the tensile properties of the spun filaments, samples were left to condition at room temperature for 48 h. The tensile properties of the filaments were measured on an Instron 3369 using a 1 kN load cell at a cross head speed of 50 mm/min with a gauge length of 100 mm. The reported values are an average of minimum five specimens for each formulation. Cryofractured filaments were used to analyse the cross-sectional surface morphologies in a Hitachi S-3400 N scanning electron microscope (SEM). To prevent the specimens from charging during the experiment, the samples were sputter coated before being observed for the morphology. ImageJ software with a pre-calibrated scale bar was employed to measure the dispersed lignin domain sizes (50 numbers) in the blend.

2.4. Thermostabilization and carbonization of the spun filament precursor fibres

The samples were thermally stabilised using an oven (Leader Engineering, UK) as shown in Fig. 2 (a). The oven was equipped with a programmable Eurotherm 3216 proportional–integral–derivative (PID) controller. The produced TcC/PA1010_50/50_2phr_MA and uncompatibilized TcC/PA1010_50/50 filament precursor bundles were cut 30 cm in length and held together using thermal tape on either end. The fibre bundles were vertically hung and fastened on an oven rack using tape. An optimal weight (2g), paper clips, were used to simulate tension to the vertically suspended bundles. The thermostabilization was conducted at two different temperatures (180 °C and 250 °C) under atmospheric conditions (Fig. 2 (c)). In the first step, the samples were isothermally thermostabilized at 180 °C for 1 h after being heated from room temperature to 180 °C with a heating rate 0.25 °C/min. Subsequently, the samples were heated to 250 °C with a heating rate of 0.25 °C/min and kept at 250 °C for 2 h to thermally stabilize the filament precursor fibre.

A temperature-controlled tube furnace (Protherm, UK) was utilized for the carbonization process and thee carbonization was carried out as shown in Fig. 2 (b). The tube furnace was equipped with a 2.5 cm internal diameter quartz tube, with airtight, swage-fitting caps placed at either end. An inlet and outlet valve on either end permitted a flow of nitrogen gas to purge the system (to prevent air ingress) from one end and the other to prevent a back flow of evolving gases during the

Table 1
Formulations prepared in melt extrusion and pilot-scale melt spinning.

Samples	TcC (wt. %)	PA1010 (wt. %)	MA (phr)[a]	GMA (phr)[a]
TcC/PA1010_50/50	50	50	–	–
TcC/PA1010_50/50_1 phr[a]_MA	50	50	1	–
TcC/PA1010_50/50_2 phr_MA	50	50	2	–
TcC/PA1010_50/50_3 phr_MA	50	50	3	–
TcC/PA1010_50/50_1 phr_GMA	50	50	–	1
TcC/PA1010_50/50_2 phr_GMA	50	50	–	2

[a] phr = parts per hundred.

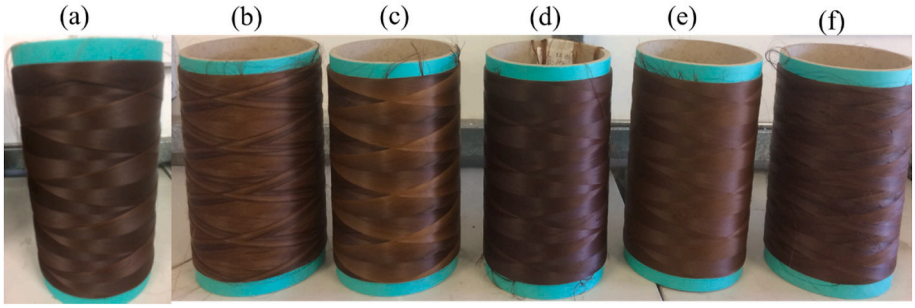

Fig. 1. Continuously spooled filaments: (a) TcC/PA1010_50/50, (b) TcC/PA1010_50/50_1phr_MA, (c) TcC/PA1010_50/50_2phr_MA, (d) TcC/PA1010_50/50_3phr_MA, (e) TcC/PA1010_50/50_1phr_GMA, and (f) TcC/PA1010_50/50_2phr_GMA.

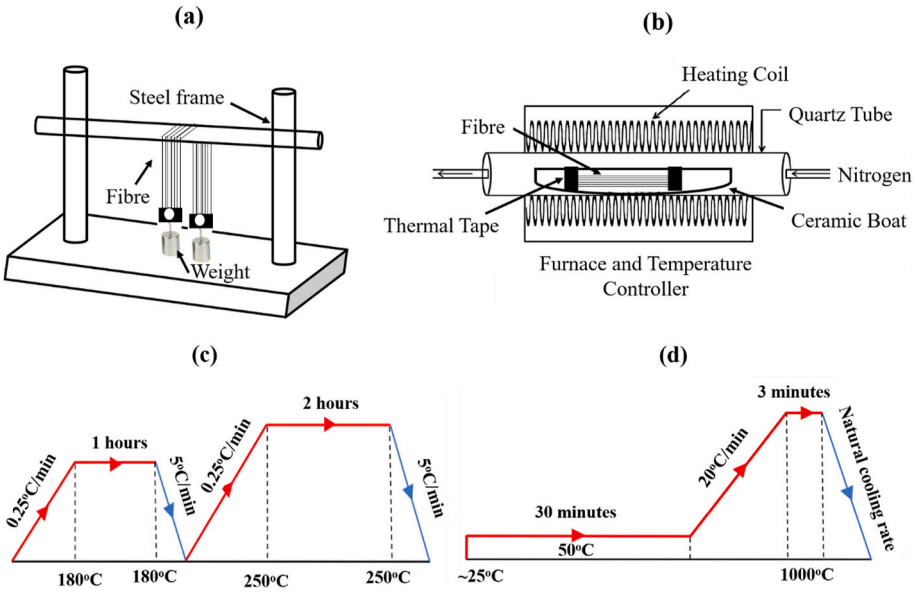

Fig. 2. Experimental setup and heating protocol for thermostabilization (a&c) and carbonization (b&d).

experimental procedure. The thermally stabilised bundles were cut to a desirable length of 20 cm with either end fixed to ceramic boats. The ceramic boat holding the sample was placed centrally into the quartz tube, which was pre-heated to 50 °C prior to the airtight swage-fitting caps being fixed to either end. A nitrogen flow of 10 cc/min into the closed system purged residual air out for 30 min at 50 °C prior to the carbonization procedure initiating at 1000 °C with a heating rate of 20 °C/min for 3 min (Fig. 2 (d)). Subsequently, the carbonized samples were cooled to room temperature.

2.5. Characterisation of the thermally stabilised and carbonized filaments

To confirm the degree of thermostabilization/thermo-oxidative crosslinking of the filaments, a detailed thermal analysis was carried out in differential scanning calorimetry, DSC, (Q2000 DSC, TA instruments) as well as thermogravimetric analysis (TGA) (SDQ-Q600, TA instruments). DSC analysis was performed on the thermostabilized filaments (~5–10 mg) by recording heat/cool cycles. The heating cycle was performed from 0 °C to 250 °C with a heating rate of 5 °C/min under nitrogen atmosphere. Subsequently, the samples were cooled to room temperature with a heating rate of 10 °C/min. The change in thermal stability and char yield of the thermostabilized filaments were analysed by TGA using around 10 mg sample masses. The TGA analysis was conducted from room temperature to 900 °C with a heating rate of 20 °C/min under nitrogen flow rate of 100 mL/min. The morphology of the thermostabilized as well as carbonized filament was analysed using a Hitachi S-3400 N scanning electron microscope (SEM). The specimens were placed vertically in the SEM sample holder to observe the cross-section morphology. The tensile properties of the carbonized fibres were tested according to BS ISO 11566:1996/JIS R 7606:2000 standard in Instron 3369 with a 100 N load cell and a gauge length of 25 mm. The tensile test of the carbonized filaments was carried out with a crosshead speed of 1 mm/min. The tensile modulus was calculated from the initial linear proportion of the stress-strain curve. The reported values are averages of at least five replicates for each sample.

3. Results and discussion

3.1. Chemical interaction between the blend components

The chemical interactions and the influence of MA and GMA compatibilizers in the TcC/PA1010 blends were investigated by FTIR spectroscopy. Fig. 3(a) and (b) shows the FTIR spectra of MA, GMA, PA1010, TcC and TcC/PA1010 blend with and without MA and GMA compatibilizer. For MA, two characteristic peaks were observed at 1734 and 1781 cm^{-1} which are assigned to symmetric C═O stretching of maleic anhydride [26–28]. GMA showed a characteristic peak at 1735 cm^{-1} for C═O stretching and a peak at 911 cm^{-1} for epoxy groups [29]. A detailed FTIR spectra of PA1010, TcC and TcC/PA1010 blends were reported in earlier publications [9,10]. In brief, the peaks at 1633 and 1536 cm^{-1} in PA1010 spectra were attributed to the amide I (C═O) and amide II (N–H), respectively. The characteristic peaks of lignin (TcC)

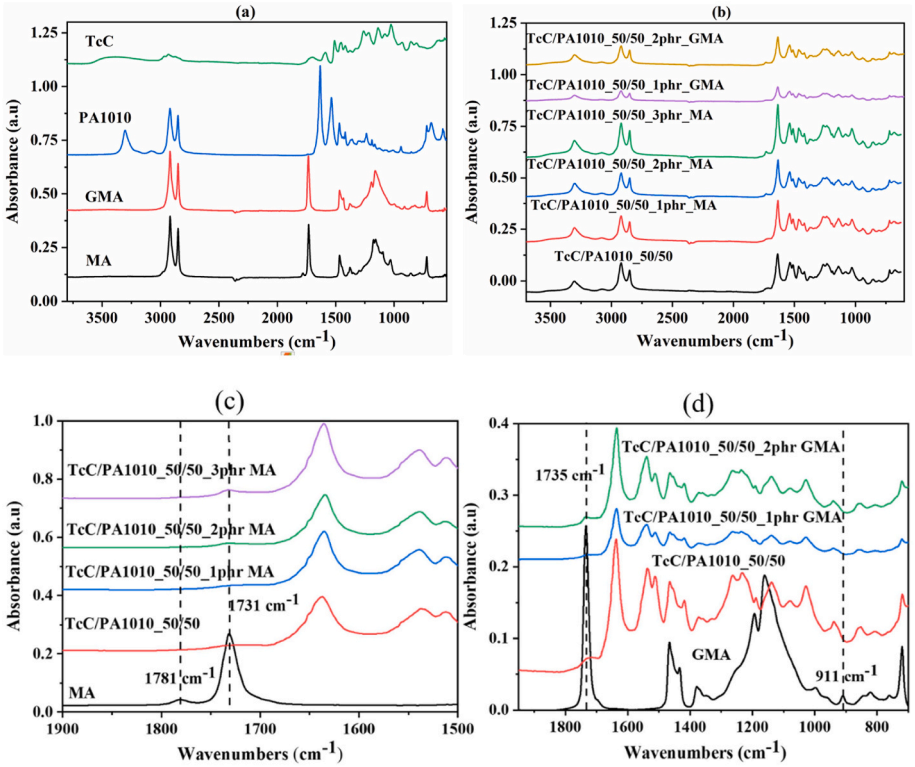

Fig. 3. FTIR spectra of MA, GMA, PA1010, TcC and their blends (a and b) and normalized absorbance spectra of compatibilizer and their corresponding blends (c and d).

were observed at 1695 cm^{-1} (aldehydes and carboxylic acid) and 1217 cm^{-1} (ether bonds). Due to intermolecular interaction between the PA1010 and TcC, TcC/PA1010 blend showed shifts in the TcC and PA1010 characteristic peaks [9]. However, TcC/PA1010 blend with MA compatibilizer (1, 2 and 3 phr) did not show any difference in the FTIR spectra compared to TcC/PA1010. It can be noted in Fig. 3(c) (normalization with respect to the maximum intensity peak of the reference MA and GMA sample spectrum) that the peak at 1781 cm^{-1} (C═O group) for the MA disappeared in the TcC/PA1010 blend with MA, indicating that the MA terpolymer had reacted with hydroxyl groups in the TcC and amine groups in the PA1010 during melt processing via *in situ* reactions [30]. Similarly, the epoxy group peak (911 cm^{-1}) of the GMA terpolymer was not detected in the FTIR spectrum (Fig. 3 (d)) of TcC/PA1010 blend with GMA (1 and 2 phr), which reflected the reactivity of epoxy groups with hydroxyl groups in the TcC and amine groups in the PA1010 [29,31]. Thus it is concluded that TcC hydroxyl groups and PA1010 amine groups can effectively react with maleic anhydride groups in the MA terpolymer as well as epoxy groups

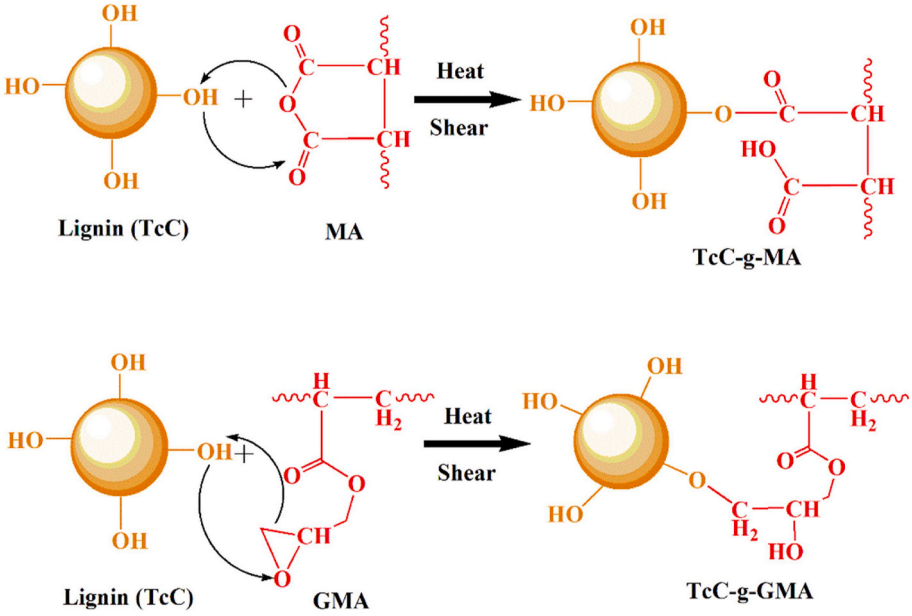

Scheme 2. Mechanism of reactivity between TcC with MA and GMA to form a covalent bond.

in the GMA compatibilizer via nucleophilic substitution to improve interfacial adhesion of the resulting blends, as shown in Scheme 2.

3.2. Thermophysical properties

3.2.1. Rheological properties

In order to understand the shear induced flow behaviour of the multiphase blends, dynamic viscoelastic measurements were conducted on the blend components (PA1010, TcC, MA and GMA) as well as TcC/PA1010 blend pellets with different compatibilizer (MA and GMA) contents as functions of frequency (Fig. 4(a) and (b)). As can be seen in Fig. 4(a) all the samples exhibited non-Newtonian shear flow behaviour for the entire tested frequency range because of the more polymer chain entanglement. The observed higher viscosity in PA1010 was due to its higher molecular weight whereas the low molecular weight and flexible linkages (e.g., ether and aliphatic chains) in TcC lignin lead to a generally overall lower viscosity [32]. As observed in Fig. 4(a), the MA and GMA show a similar viscosity trend. Owing to the lower viscosity of TcC, the TcC/PA1010 blend had low viscosity compared to PA1010. From Fig. 4(b), the complex viscosity of the TcC/PA1010 blends with MA compatibilizer (1, 2 and 3 phr) were higher, especially at a lower frequency range. This difference may be attributed to the restricted polymer chain mobility caused by *in situ* reaction of PA1010 and TcC with MA compatibilizer [14]. It is worth noting that the TcC/PA1010 blend in the presence of 2 ph MA showed the highest general viscosity increase. This could be related to an optimal compatibilizer concentration, which leads to the greatest compatibility between the PA1010 and TcC. Moreover, the optimal MA content (2 phr) could facilitate more chain entanglement to enhance the shear-thinning behaviour at higher frequencies by chain rupture. Regarding the GMA compatibilizer, there is a slight increase in viscosity at lower frequencies for the TcC/PA1010 blend in the presence of 1 phr GMA, indicating improved compatibility between PA1010 and TcC (Fig. 4(b)). However, when the GMA content was increased to 2 phr, a significant viscosity reduction is observed. This is most likely because 1 phr GMA was sufficient to reduce the lignin domain size for TcC/PA1010 blend, as evidenced by change in lignin domain size observed by SEM (see Section 3.5). Higher GMA levels (2 phr) will increase the mobility of GMA macromolecules thus reducing the blend viscosity. Similar observations have been reported in the lignin blends in the presence of styrene-ethylene/butylene-styrene-maleic anhydride-grafted compatibilizer [14]. The observed optimal reactivity of the TcC/PA1010 with 2 ph MA or 1 phr GMA could be useful to produce the filaments with ease.

3.2.2. Glass transition temperatures

Glass transition temperature (T_g) of the TcC powder, PA1010 pellets and their blend pellets were measured by DMA (Table 2). Both TcC and PA1010 showed single T_g values at 133 °C and 57 °C, respectively whereas two T_g values (81 and 145 °C) were observed for TcC/PA1010 blends. These latter suggest that TcC and PA1010 are not fully miscible at the molecular level. The addition of compatibilizer into TcC/PA1010 blend leads the T_g value of both the TcC phase and PA1010 phases to come close to each other. The overall T_g value increase was about 20 °C for the PA1010 component while about 9 °C decrease for the TcC component relative to the respective component values in the uncompatibilized blend, which is evidence of the enhanced interfacial interaction in the presence of compatibilizers [33,34]. These results are in good agreement with the observations made in the FTIR spectral changes in Fig. 3.

3.2.3. Melting and recrystallisation properties

DSC results of PA1010 and TcC/PA1010 blend pellets with and without compatibilizer are shown in Fig. 5 and derived data summarized in Table 2. According to the manufacturer's technical data sheets, the melting points of the MA and GMA terpolymers are both about 65 °C. Bimodal melting points were observed for PA1010 [10], which are directly associated with γ-crystalline (190 °C) and α-crystalline (198 °C) phases present [35]. The more intense, γ – phase melting endotherm of PA1010 was reduced in intensity and appeared as a shoulder after the addition of TcC and shifted from 190 °C to 185 °C, indicating a degree of compatibility between the PA1010 and TcC [9]. The further addition of MA and GMA showed no further changes in the melting temperatures of PA1010 except for the blend with 2 ph MA, which had three distinguishable melting peaks. These three melting peaks are attributed to the γ-form (184 °C), β-from (188 °C) and α-form (194 °C) crystal formation [36]. This observed extra melting peak for the 2 ph MA condition, could also be made of small mesomorphic aggregates of PA1010 chains when there is good compatibility achieved [37].

The dominance of the α-form in the TcC/PA1010 blends regardless of the MA and GMA content has been observed previously in other polyamide ternary blends [38]. In addition to the effect of compatibilization is that of the influence of blend component and compatibilizer on PA1010 nucleation. Table 2 shows that the crystallization temperature (T_c) of the PA1010 was reduced from 177 to 173 °C in the presence of TcC because of the heterogeneously nucleated crystallization. However, the T_c value of PA1010 in the TcC/PA1010 blend with MA and GMA was the same as for PA1010 alone. The heterogeneously nucleated crystallization is most likely responsible for the observed increase of the crystallinity percentage of PA1010 in the TcC/PA1010 blend (Table 2). On the other hand, PA1010 crystallinity was reduced when MA or GMA was introduced into TcC/PA1010 blend, suggesting that the effect of heterogeneous nucleation is reduced as the TcC domain size is reduced. This is corroborated by SEM images (see Section 3.5) where the fine dispersion of TcC domains was observed.

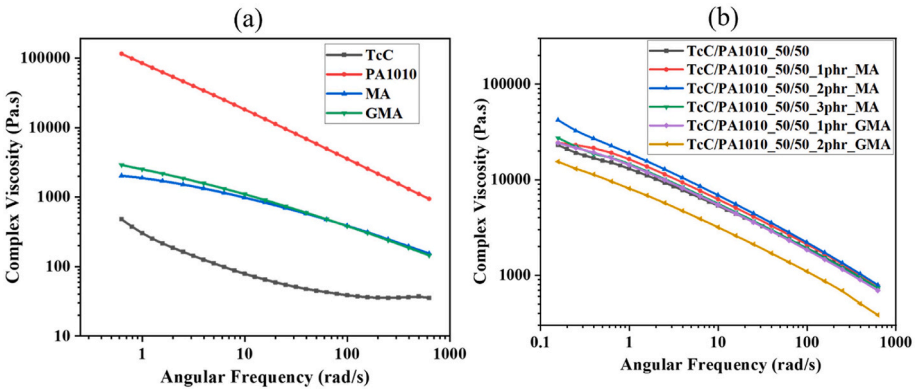

Fig. 4. Complex viscosity of (a) PA1010, TcC, MA, GMA, and (b) TcC/PA1010_50/50 blend with and without MA and GMA.

Table 2
Thermophysical transitions from DMA and DSC responses for PA1010, MA, GMA and TcC/PA1010 blends with and without MA and GMA.

Samples	DMA	DSC			
	T_g (°C)	Melting point, T_m (°C)	Melting enthalpy (J/g)	Crystallization temperature, T_c (°C)	Crystallinity (%)
TcC	133	–	–	–	–
PA1010	57	190, 198	97.1	177	39.8
TcC/PA1010_50/50	81, 145	185, 196	62.8	173	51.5
TcC/PA1010_50/50_1phr_MA	101, 136	186, 195	55.9	177	45.8
TcC/PA1010_50/50_2phr_MA	101, 136	184, 188, 194	45.9	178	37.6
TcC/PA1010_50/50_3phr_MA	101, 136	187, 195	52.3	178	42.8
TcC/PA1010_50/50_1phr_GMA	104,138	186, 195	55.9	177	45.8
TcC/PA1010_50/50_2phr_GMA	103, 136	185, 195	48.8	176	40.0

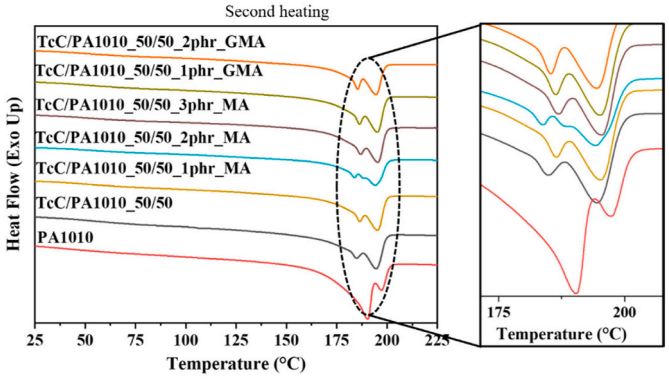

Fig. 5. DSC thermogram of TcC/PA1010 blends in the presence and absence of MA and GMA along with magnified PA1010 melting region.

3.3. Effect of compatibilizers on blend melt processability and derived filaments

3.3.1. Thermogravimetric analysis

Prior to melt spinning the compounded blended pellets into filaments, a thermogravimetric analytical (TGA) study was performed to study the effect of compatibilizers on blend stability, which could help in setting up the appropriate extruder parameters. The TGA profiles shown in Fig. 6 and the important derived parameters, namely onset of degradation (taken as temperature where 5% mass loss occurs), $T_{5\%}$ and maximum degradation (as the derivative thermogram (DTG) peak maximum), T_{max}, temperatures reported in Table 3 indicate that there is

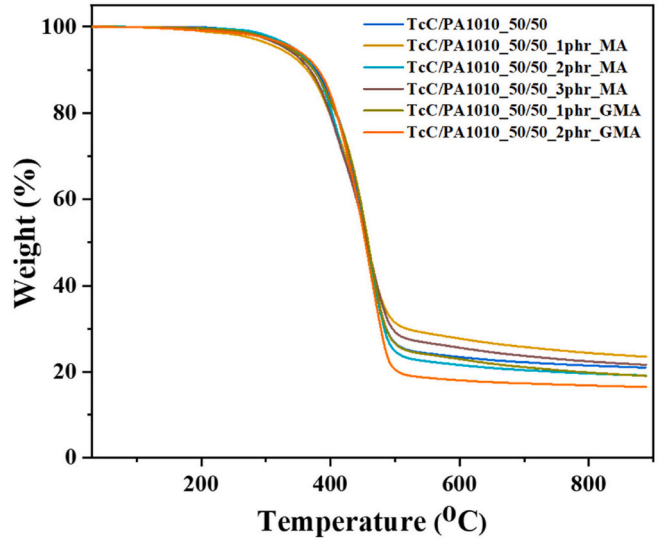

Fig. 6. TGA cures of the compatibilized and uncompatibilized blends.

Table 3
Summary of thermogravimetric analysis.

Samples	$T_{5\%}$ (°C)	T_{max} (°C)	Char residue (%) at 600 °C	Char residue (%) at 880 °C
TcC/PA1010_50/50	398	457	23	21
TcC/PA1010_50/50_1phr_MA	386	454	28	24
TcC/PA1010_50/50_2phr_MA	395	463	22	19
TcC/PA1010_50/50_3phr_MA	383	463	26	22
TcC/PA1010_50/50_1phr_GMA	403	461	23	19
TcC/PA1010_50/50_2phr_GMA	399	463	18	17

a minimal detrimental effect of the compatibilizers in terms of any changes in thermal degradation that can affect the processing. The residual char levels at 600 °C are considered to be initial char levels following the main preceding volatilisation stage and those at 880 °C are for more fully developed chars, which still show small variations although no simple dependence on blend type is evident. Hence, similar processing parameters were used for all samples. After melt extrusion of all blend formulations, it was observed that the lowest filament diameters (50–80 μm) were achieved from the compatibilized TcC/PA1010 blends, which suggests that both MA and GMA had significantly influenced melt processability in a positive manner (see below). However, while the TcC/PA1010 blends with 1, 2 and 3 ph MA as well as 1 and 2 phr GMA showed superior and uninterrupted melt spinning properties, that containing 3 phr GMA was difficult to process into acceptable filaments because of the change in melt flow behaviour. Hence, the TcC/PA1010 blend with 3 phr GMA was not investigated further.

3.3.2. Tensile properties of the melt spun filaments

Rheological properties (Fig. 4(b)) and T_g changes (Table 2) in the TcC/PA1010 with 2 ph MA or 1 phr GMA showed the optimal compatibility, therefore, such blends are expected to produce filaments with improved tensile properties compared to corresponding compatibilized blends. Typical tensile stress-strain curves are presented in Fig. 7 (a) for PA1010 and TcC/PA1010 blends with different concentration of MA and GMA. Unlike PA1010, TcC/PA1010 and TcC/PA1010 with MA and GMA exhibited clear yield stresses indicating a ductile failure. Only TcC/PA1010 with 2 ph MA blend showed higher breaking stress than respective yield stress value. This effect could be caused by uniform distribution of β-crystals in the tensile axis, leading to strain hardening behaviour [39]. The average tensile strength and tangent modulus values of the PA1010 and TcC/PA1010 with and without MA/GMA are depicted in Fig. 7(b). The blending of TcC with PA1010 has resulted in a reduction in tensile strength of the latter because of the limited compatibility between them, while the lignin domains act as reinforcement at room temperature thus increasing the modulus with respect to 100% PA1010. This reinforcing effect is caused by the rigid

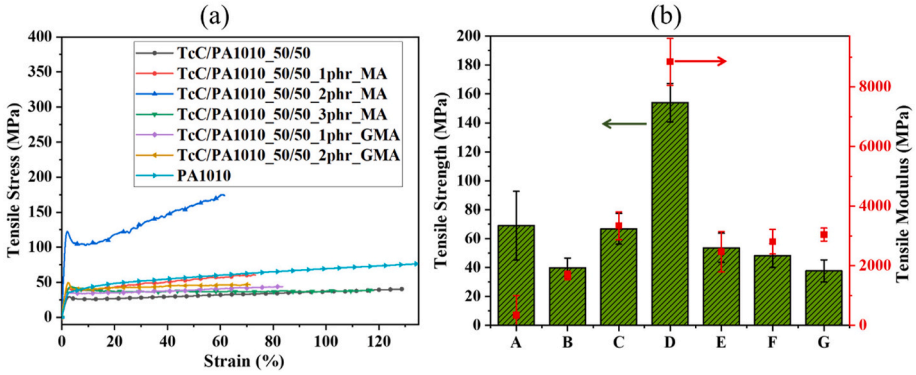

Fig. 7. (a) Tensile stress-strain curves for PA1010 and TcC/PA1010 blends with and without MA/GMA; (b) average tensile strength and modulus: (A) PA110, (B) TcC/PA1010_50/50, (C) TcC/PA1010_50/50_1phr_MA, D) TcC/PA1010_50/50_2phr_MA, (E) TcC/PA1010_50/50_3phr_MA, (F) TcC/PA1010_50/50_1phr_GMA and (G) TcC/PA1010_50/50_2phr_GMA.

phenolic functionality in TcC and spherical TcC particles dispersed in the PA1010 phase (see SEM images, section 3.3.3) [32]. The TcC/PA1010 blend modulus was improved further in the presence of MA/GMA because of the enhanced uniform dispersion of TcC, enhanced interfacial interaction, and effective stress transfer between the PA1010 and TcC phases. Similarly, the enhanced interfacial interaction leads to increase in the tensile strength of TcC/PA1010 blends containing either MA or GMA. A maximum tensile strength (154 MPa) and modulus (~8.8 GPa) improvement were observed in the TcC/PA1010 blend with 2 ph MA. As mentioned earlier, it is possible that the β-crystal orientation in the tensile axis is reason for the high strain hardening effect in the TcC/PA1010 blend with 2 ph MA, thus leading to high strength [30]. The compatibility between the blended components has a strong influence on formation of the β-crystals during stretching. As seen above by rheological and T_g studies, the optimal compatibility between the PA1010 and lignin was achieved with the incorporation of 2 ph MA, and β-crystal formation was also indicated by the DSC study. It could be possible that PA1010 in the TcC/PA1010_50/50_3phr_MA blend forms α and β-crystals stable at room temperature, with the latter not being stable at higher temperatures. Unlike blends with 1 or 3 ph MA, that containing 2 ph MA showed the presence of thermodynamically stable α and β-crystals following DSC analysis. It has also been reported in the literature that polyamide 6 with β-crystals could be obtained by uniaxially stretching, which induced the α-to-β transformation [37,40]. Thus the optimal compatibilized blend can hold the arranged zigzag conformations within the crystallites by means of the intermolecular interaction, leading to the stable β-polymorph form, which provides high tensile strength and modulus compared to PA1010/lignin compatibilized with 1 or 3 ph MA blends. The TcC/PA1010 blend with 2 phr GMA had lower tensile strength than their MA-containing analogues. This phenomenon could explain that the GMA is less efficient as a compatibilizer compared to MA. Similarly, GMA presence shows a lower effect than MA in terms of T_g changes with respect to neat PA1010.

3.3.3. Morphologies of the melt spun filaments

Surface and cross-sectional morphologies of the melt spun Tcc/PA1010 blend filaments with different concentrations of MA and GMA are shown in Fig. 8(a) and (b). Regardless of the blend compositions, all the filaments have smooth and uniform surface morphologies with diameter of around 110 μm (Fig. 8(a)). Cross-sectional images of the filament were used to study the phase behaviour of the blend as shown in Fig. 8(b). The observed generally heterogenous morphology of the TcC/PA1010 blend with and without MA or GMA suggests that TcC and PA1010 are not miscible at the molecular level. A co-continuous phase separation morphology can be seen in the TcC/PA1010 blend with no compatibilizer with TcC phase segregation appearing as globular particles (Fig. 8(b) (i)). On the contrary, a less discontinuous phase blend was evident in blends with either MA or GMA. Such morphological changes in the blend are attributed to the enhanced interaction between the compatibilized, blended components as mentioned earlier. The enhanced interaction also reduced the apparent diameters of TcC particles in the PA1010 phase. Despite all the samples having been cryo-fractured, the TcC/PA1010 with 2 ph MA (Fig. 8(b)(iii) and 2 phr GMA (Figure (b)(vi) showed relatively more ductile deformation. Such a deformation could be due to the good interfacial interaction between TcC and PA1010, which could prevent crack initiation and propagation by facilitating effective stress transfer during the fracture process [41]. Table 4 depicts the average TcC particle size with standard deviation in the PA1010 matrix with and without compatibilizer. The average TcC particle size (1.1 ± 0.10 μm) in the uncompatibilized TcC/PA1010 blend is much higher compared to compatibilized TcC/PA1010 blend because of TcC aggregation. However, the average TcC particle size between the various compatibilized blends did not show a significantly large differences compared to the much larger differences with respect to the uncompatilized blend. However, the variances of the TcC average particle size between the latter and compatibilized blends are significantly different. These could be explained by assuming they are spherical during measurement without considering the elongated particles during fracture. The blends prepared with 2 ph MA or GMA compatibilizers especially showed large variances, which could be partly due to reduced crack initiation and propagation during the fracture caused by the enhanced interfacial interaction between TcC and PA1010.

3.4. Thermally stabilised and carbonized filaments

Since these filaments are to be used as precursors for carbon fibre production, carbon yield is quite important besides producing carbon fibres with defect free and compact structure [7]. In our previous work, TcC/PA1010_50/50 filaments were produced in a lab-scale melt spinning extruder (Labline MK 1) and thermostabilized under a simulated thermostabilization condition using thermogravimetric analyser [9]. It was observed that the char yield of the thermostabilized TcC/PA1010_50/50 filament was around 34%, which is low compared to polyacrylonitrile (PAN)-based carbon fibre precursors. Therefore, an improved precursor filaments preparation and thermostabilization protocol was used as described in Sections 2.1 and 2.4 to achieve a higher char yield in the thermostabilized TcC/PA1010 filaments. Compatibility of the lignin with the blending partner is one of the factors which can influence the carbon yield as well as performances of the lignin derived carbon fibres [42,43]. Therefore, uncompatibilized filaments (TcC/PA1010_50/50) and one of the optimal compatibilized blend filaments (TcC/PA1010_50/50_2phr_MA) were selected for the simulated thermal stabilization and carbonization processes to evaluate the potential of carbon fibre production.

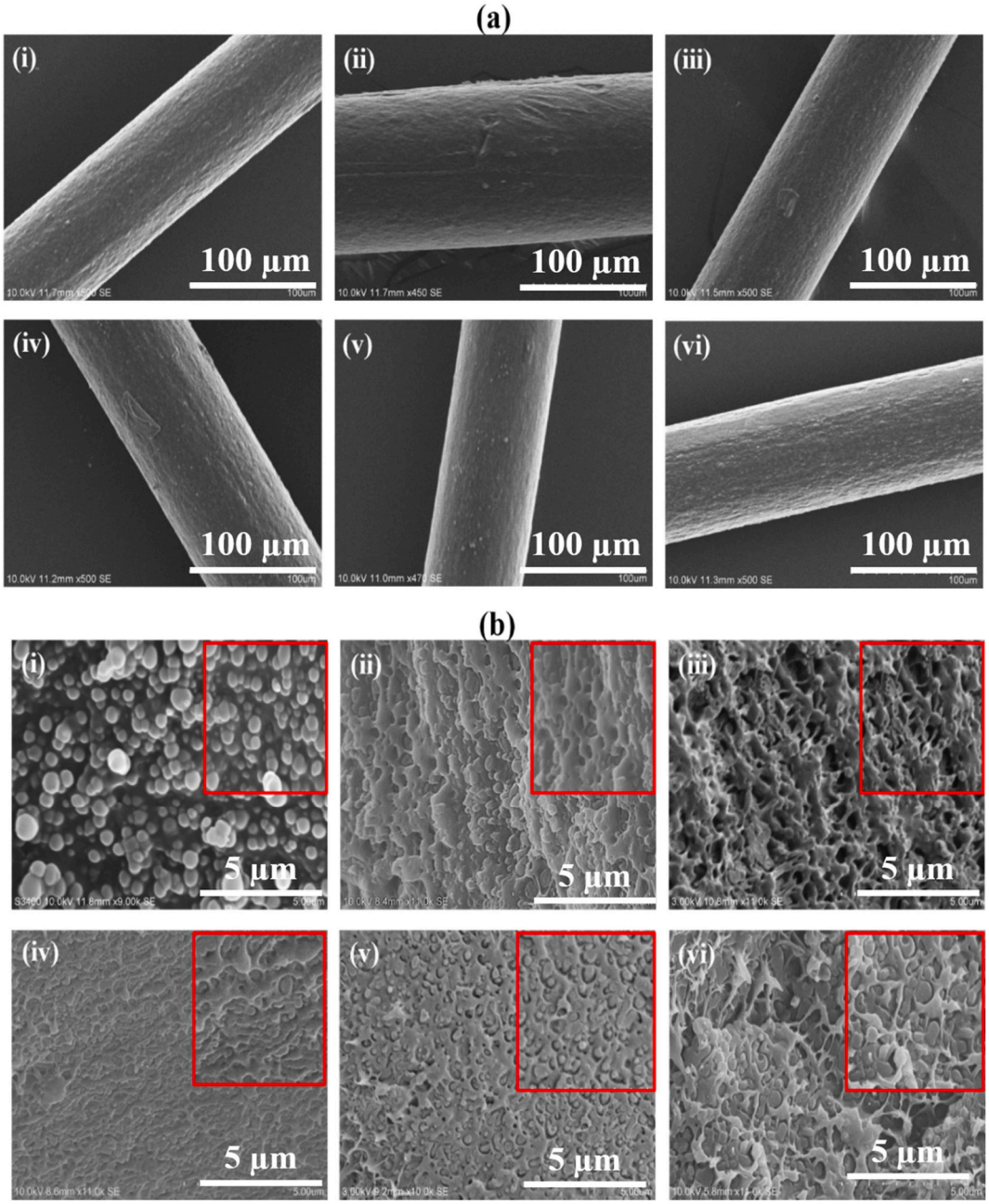

Fig. 8. (a) Surface morphology of the filaments: (i) TcC/PA1010_50/50, (ii) TcC/PA1010_50/50_1phr_MA, (iii) TcC/PA1010_50/50_2phr_MA, (iv) TcC/PA1010_50/50_3phr_MA, (v) TcC/PA1010_50/50_1phr_GMA, and (vi) TcC/PA1010_50/50_2phr_GMA; (b) Cross-sectional morphology of the filament (insert is magnified image): (i) TcC/PA1010_50/50, (ii) TcC/PA1010_50/50_1phr_MA, (iii) TcC/PA1010_50/50_2phr_MA, (iv) TcC/PA1010_50/50_3phr_MA, (v) TcC/PA1010_50/50_1phr_GMA, and (vi) TcC/PA1010_50/50_2phr_GMA.

Table 4
Lignin (TcC) average particle size (measured in the red square areas in Fig. 9 (b)) in PA1010 matrix with and without compatibilizer.

Sample	Average TcC particle size in PA1010 matrix (µm)
TcC/PA1010_50/50	1.1 ± 0.10
TcC/PA1010_50/50_1phr_MA	0.53 ± 0.09
TcC/PA1010_50/50_2phr_MA	0.64 ± 0.26
TcC/PA1010_50/50_3phr_MA	0.71 ± 0.18
TcC/PA1010_50/50_1phr_GMA	0.65 ± 0.14
TcC/PA1010_50/50_2phr_GMA	0.89 ± 0.27

3.4.1. Thermal analysis of the thermostabilized filaments

After thermal stabilization, which is assumed to involve thermo-oxidative crosslinking, the filaments were quite flexible, without fusing together. The diameters of the filaments were reduced from 102-127 µm to 56–80 µm while their average lengths increased from 30 to 45 cm (i.e., 33%) after thermostabilization. The observed changes in the filament diameter and length are attributed to the tension applied on the filaments during thermostabilization. The changes in thermal events of the thermostabilized filaments were analysed by DSC and TGA. The second heating and first cooling DSC thermograms of the thermo-stabilized and corresponding unstabilized filaments are shown in Fig. 9 (a) and (b). DSC thermograms showed that thermostabilized filaments did not show any melting behaviour with absence of PA1010 fusion

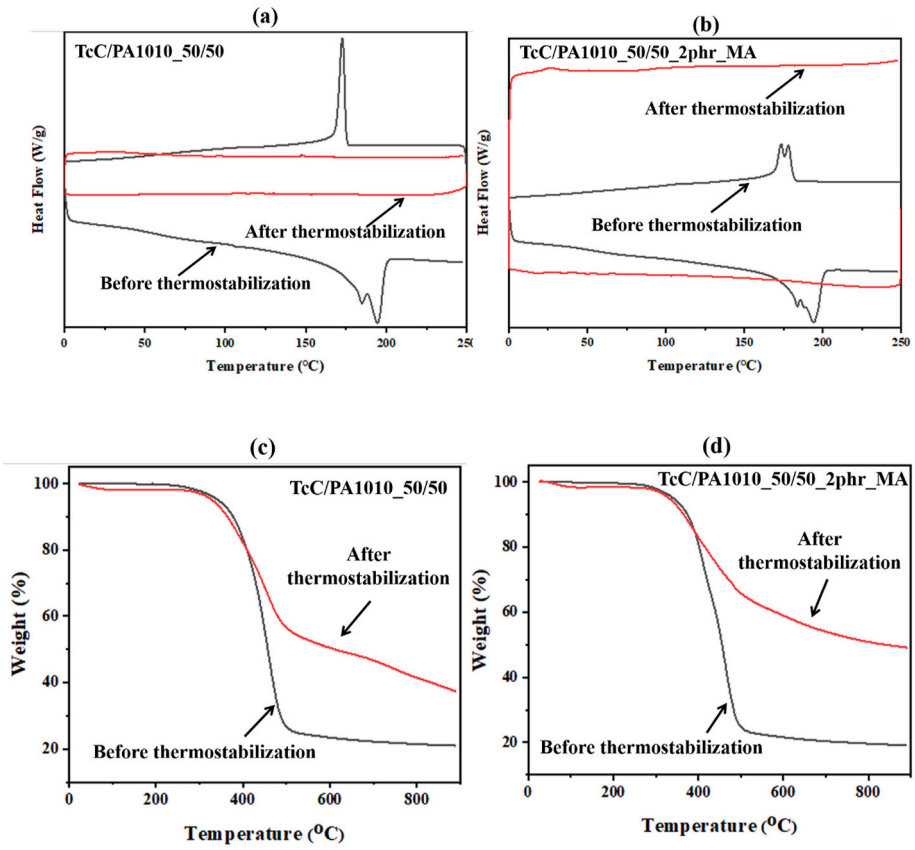

Fig. 9. DSC (a and b) and TGA (c and d) thermograms of the filaments before and after thermostabilization.

endothermic peaks, indicating that cross-linking had occurred between the component lignin and polyamide chains. Fig. 9 (c) and (d) shows the TGA responses of the filaments before and after thermal stabilization, which show that the char yield of the thermostabilized filament was higher compared to their corresponding as-spun filaments. Similar phenomena was observed in a previous study [9]. These increased char yields are most likely be due to the dehydration, condensation, cross-linking and elimination reactions of lignin accompanied by water, CO and CO_2 release through the formation of ketone, ester and anhydride linkages during thermal stabilization at 250 °C [24] coupled with lignin-PA1010 cross-linking reactions. Notably, the char yield of the thermostabilized TcC/PA1010_50/50_2phr_MA filaments was determined to be ~49.5% at 850 °C, which is significantly higher compared to thermostabilized TcC/PA1010_50/50 filaments (43.0%). These improved char yields in compatibilized blends suggest that the presence of MA has increased the cross-linking interactions between the components thereby causing higher carbon yields.

3.4.2. *Morphological and mechanical properties of the thermally stabilised and carbonized filaments*

Fig. 10 shows the cross-sectional morphology of the thermostabilized and carbonized filaments. Unlike thermostabilized TcC/PA1010_50/50_2phr_MA filaments (Fig. 10 (e and f)), thermostabilized TcC/PA1010_50/50 filaments showed the presence of micro voids as shown in Fig. 10 (a) and (b), most likely a consequence of the blend heterogeneity. The diameter ranges for the carbonized TcC/PA1010_50/50

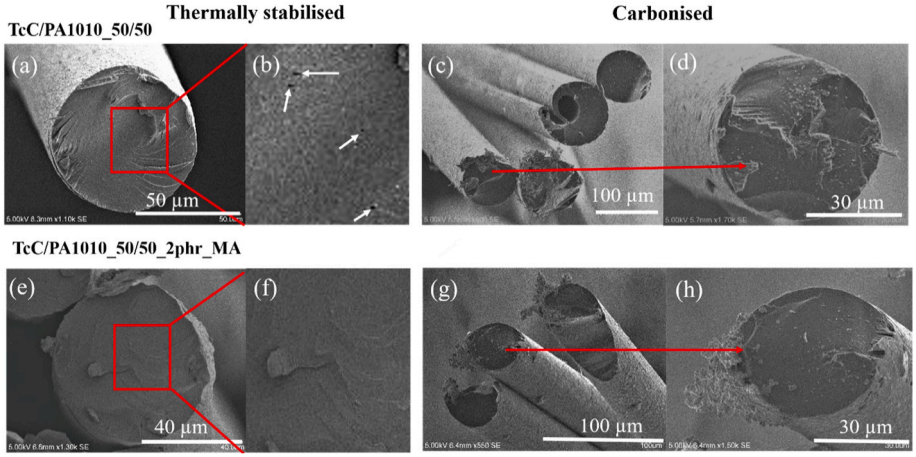

Fig. 10. SEM cross-sectional morphology of the thermostabilized and carbonized TcC/PA1010_50/50 and TcC/PA1010_50/50_2phr_MA filaments.

and TcC/PA1010_50/50_2phr_MA filaments were 42–54 μm and 40–50 μm, respectively (Fig. 10 (c, d, g, and h)). The carbonization of the filament leads to weight loss as well as shrinkage in the filament length [44]. During carbonization with no load applied on the filaments, a shrinkage of 24% was noted for both carbonized filaments. In general, the length changes may be said to follow a behaviour typical of carbonization processes [45]. While some of the carbonized TcC/PA1010_50/50 filaments showed larger voids as can be seen in Fig. 10 (c), the cross-sectional morphologies of the carbonized TcC/PA1010_50/50_2phr_MA filaments (Fig. 10 (g) and (h)) clearly display a more homogeneous morphology with absence of detrimental porosity.

Table 5 shows the tensile properties of the carbonized TcC/PA1010_50/50 and TcC/PA1010_ 50/50_2phr_MA filaments. Both samples exhibited brittle fracture with a low percentage of elongation (0.5–2.4%), which is similar to traditional carbon fibre filament fracture. Carbonized TcC/PA1010_50/50 filaments showed an average modulus of 16.2 ± 2.2 GPa while carbonized TcC/PA1010_50/50_2phr_MA filaments showed modulus of 13.9 ± 1.7 GPa. The average tensile stress of the carbonized TcC/PA1010_50/50 and TcC/PA1010_50/50_2phr_MA filament were 192 ± 77 and 159 ± 95 MPa, respectively. These slightly inferior results for the carbonized filaments are surprising since MA compatibilized precursor blend (TcC/PA1010_50/50_2phr_MA) showed a less discontinuous phase morphology in the precursor filaments and enhanced char yield compared to the uncompatibilized blend. However, crucial to the development of carbon fibres having acceptably high tensile properties, is the need to control stress application during both thermostabilization and carbonization processes [46]. Under the experimental conditions used here, fine control of stress during both stages has not been possible and in any case because of the different rheological differences observed between compatibilized and un compatibilized blends, each respective precursor filament would most likely require a different stress profile during conversion to final carbon fibres having optimal tensile properties. Whether or not the presence of a compatibilizer that gives enhanced precursor properties leads to superior carbon fibres would depend on the outcome of further research in this area.

Compared to commercial PAN-based carbon fibres (4.85 GPa tensile stress and 220 GPa tensile modulus) [47] the values of TcC/PA1010_50/50 and TcC/PA1010_ 50/50_2phr_MA carbon filaments are much lower. Similar results were seen for carbon fibres produced from lignin/TPU (thermoplastic elastomer polyurethane) precursor fibres by Culebras et al. [42]. Commercial PAN-based precursor fibres (6.3 μm diameter) are thermally stabilised and carbonized in a continuous process, where the fibre is kept under tension, resulting in carbon fibre with 5–7 μm diameter [47,48]. Also, it is reported that the small diameters of the filaments allowed formation of homogeneous microstructure across the diameter in the resulting carbon fibres [47]. However, in the present case the precursor fibres were extruded using FET pilot extruder line, with fibre diameter being 50–80 μm; thermal stabilization was carried out in vertical orientation with minimal tension and during carbonization process while the fibre was held horizontally, the tension was minimal. This work though has shown the potential of producing carbon fibres from lignin/PA1010 blends and it is envisaged that with improved processing parameters, carbon fibres with improved mechanical properties can be obtained.

4. Conclusions

This work has demonstrated that continuous melt spinnability of lignin (TcC)/PA1010 (50/50 wt%) blend with and without compatibilizer using sup-pilot scale melting spinning process was successful. In the presence of MA and GMA-based compatibilizers, the compatibility between the lignin (TcC) and PA1010 was improved, demonstrated by the inclusion phase domain size reduction in compatibilized blends compared to the uncompatibilized counterpart. However, the compatibilizer concentrations played an important role to achieve an optimal performance in the resulting blends. While 2 phr MA- and 1 phr GMA-based compatibilizers showed good results, the former was more effective in producing filaments with good mechanical properties. Because both uncompatibilised and compatibilized TcC/PA1010 filaments could be successfully thermally stabilised and carbonized, this shows the potential of using this blend for carbon fibre production.

Table 5
Mechanical properties of the carbonized filaments.

Precursor	Tensile strength (MPa)	Tensile modulus (GPa)	Elongation at break (%)	Diameter (μm)
TcC/PA1010_50/50	192 ± 77	16.2 ± 2.2	1.6 ± 0.8	42–54
TcC/PA1010_50/50_2phr_MA	159 ± 95	13.9 ± 1.7	1.6 ± 0.8	40–50

Declaration of competing interest

The authors declare that they have no known competing financial interests or personal relationships that could have appeared to influence the work reported in this paper.

Acknowledgements

This work is part of the Project funded from the BioBased Industries Joint Undertaking under the European Union's Horizon 2020 research and innovation programme under Grant Agreement No. 720707.

References

[1] B. Imre, B. Pukánszky, Compatibilization in bio-based and biodegradable polymer blends, Eur. Polym. J. 49 (2013) 1215–1233, https://doi.org/10.1016/j.eurpolymj.2013.01.019.
[2] M. Palabiyik, S. Bahadur, Mechanical and tribological properties of polyamide 6 and high density polyethylene polyblends with and without compatibilizer, Wear 246 (2000) 149–158, https://doi.org/10.1016/S0043-1648(00)00501-9.
[3] S. Laurichesse, L. Averous, Chemical modification of lignins: towards biobased polymers, Prog. Polym. Sci. 39 (2014) 1266–1290.
[4] L. Mu, Y. Shi, L. Chen, T. Ji, R. Yuan, H. Wang, J. Zhu, [N-Methyl-2-pyrrolidone][C1–C4 carboxylic acid]: a novel solvent system with exceptional lignin solubility, Chem. Commun. 51 (2015) 13554–13557, https://doi.org/10.1039/C5CC04191K.
[5] D. Kun, B. Pukánszky, Polymer/lignin blends: interactions, properties, applications, Eur. Polym. J. 93 (2017) 618–641.
[6] C. Bonini, M. D'Auria, L. Emanuele, R. Ferri, R. Pucciariello, A.R. Sabia, Polyurethanes and polyesters from lignin, J. Appl. Polym. Sci. 98 (2005) 1451–1456.
[7] E. Frank, L.M. Steudle, D. Ingildeev, J.M. Spörl, M.R. Buchmeiser, Carbon fibers: precursor systems, processing, structure, and properties, Angew. Chem. Int. Ed. 53 (2014) 5262–5298.
[8] J. Wang, R.S.J. Manley, D. Feldman, Synthetic polymer-lignin copolymers and blends, Prog. Polym. Sci. 17 (1992) 611–646.
[9] R. Muthuraj, A.R. Horrocks, B.K. Kandola, Hydroxypropyl-modified and organosolv lignin/bio-based polyamide blend filaments as carbon fibre precursors, J. Mater. Sci. 55 (2020) 7066–7083, https://doi.org/10.1007/s10853-020-04486-w.
[10] R. Muthuraj, M. Hajee, A.R. Horrocks, B.K. Kandola, Biopolymer blends from hardwood lignin and bio-polyamides: compatibility and miscibility, Int. J. Biol. Macromol. 132 (2019) 439–450, https://doi.org/10.1016/j.ijbiomac.2019.03.142.
[11] S. Sahoo, M.Ö. Seydibeyoğlu, A.K. Mohanty, M. Misra, Characterization of industrial lignins for their utilization in future value added applications, Biomass Bioenergy 35 (2011) 4230–4237, https://doi.org/10.1016/j.biombioe.2011.07.009.
[12] C. Koning, M. Van Duin, C. Pagnoulle, R. Jerome, Strategies for compatibilization of polymer blends, Prog. Polym. Sci. 23 (1998) 707–757, https://doi.org/10.1016/S0079-6700(97)00054-3.
[13] W. Yang, F. Dominici, E. Fortunati, J.M. Kenny, D. Puglia, Effect of lignin nanoparticles and masterbatch procedures on the final properties of glycidyl methacrylate-g-poly (lactic acid) films before and after accelerated UV weathering, Ind. Crop. Prod. 77 (2015) 833–844.
[14] P. Song, Z. Cao, Q. Meng, S. Fu, Z. Fang, Q. Wu, J. Ye, Effect of lignin incorporation and reactive compatibilization on the morphological, rheological, and mechanical properties of ABS resin, J. Macromol. Sci. Part B. 51 (2012) 720–735.

[15] J.K. Kim, S. Kim, C.E. Park, Compatibilization mechanism of polymer blends with an in-situ compatibilizer, Polymer 38 (1997) 2155–2164.
[16] S.-C. Chen, L.-H. Zhang, G. Zhang, G.-C. Zhong, J. Li, X.-M. Zhang, W.-X. Chen, An investigation and comparison of the blending of LDPE and PP with different intrinsic viscosities of PET, Polymers 10 (2018) 147, https://doi.org/10.3390/polym10020147.
[17] G. Maglio, M. Malinconico, A. Migliozzi, G. Groeninckx, Immiscible poly(L-lactide)/poly(ε-caprolactone) blends: influence of the addition of a poly(L-lactide)-poly(oxyethylene) block copolymer on thermal behavior and morphology, Macromol. Chem. Phys. 205 (2004) 946–950, https://doi.org/10.1002/macp.200300150.
[18] D. Wu, Y. Zhang, L. Yuan, M. Zhang, W. Zhou, Viscoelastic interfacial properties of compatibilized poly (ε-caprolactone)/polylactide blend, J. Polym. Sci., Part B: Polym. Phys. 48 (2010) 756–765.
[19] R. Dell'Erba, G. Groeninckx, G. Maglio, M. Malinconico, A. Migliozzi, Immiscible polymer blends of semicrystalline biocompatible components: thermal properties and phase morphology analysis of PLLA/PCL blends, Polymer 42 (2001) 7831–7840, https://doi.org/10.1016/S0032-3861(01)00269-5.
[20] S.H. Clasen, C.M.O. Müller, A.T.N. Pires, Maleic anhydride as a compatibilizer and plasticizer in TPS/PLA blends, J. Braz. Chem. Soc. 26 (2015) 1583–1590.
[21] A.V. Maldhure, J.D. Ekhe, E. Deenadayalan, Mechanical properties of polypropylene blended with esterified and alkylated lignin, J. Appl. Polym. Sci. 125 (2012) 1701–1712.
[22] B. Bozsódi, V. Romhányi, P. Pataki, D. Kun, K. Renner, B. Pukánszky, Modification of interactions in polypropylene/lignosulfonate blends, Mater. Des. 103 (2016) 32–39.
[23] M. Pracella, M. Haque, V. Alvarez, Functionalization, compatibilization and properties of polyolefin composites with natural fibers, Polymers 2 (2010) 554–574.
[24] M. Culebras, M.J. Sanchis, A. Beaucamp, M. Carsí, B.K. Kandola, A.R. Horrocks, G. Panzetti, C. Birkinshaw, M.N. Collins, Understanding the thermal and dielectric response of organosolv and modified kraft lignin as a carbon fibre precursor, Green Chem. 20 (2018) 4461–4472, https://doi.org/10.1039/C8GC01577E.
[25] M. Yan, H. Yang, Improvement of polyamide 1010 with silica nanospheres via in situ melt polycondensation, Polym. Compos. 33 (2012) 1770–1776.
[26] R. Muthuraj, M. Misra, A.K. Mohanty, Injection molded sustainable biocomposites from poly(butylene succinate) bioplastic and perennial grass, ACS Sustain. Chem. Eng. 3 (2015) 2767–2776, https://doi.org/10.1021/acssuschemeng.5b00646.
[27] R. Muthuraj, M. Misra, A.K. Mohanty, Biocomposite consisting of miscanthus fiber and biodegradable binary blend matrix: compatibilization and performance evaluation, RSC Adv. 7 (2017) 27538–27548, https://doi.org/10.1039/C6RA27987B.
[28] R. Muthuraj, M. Misra, A.K. Mohanty, Biodegradable biocomposites from poly (butylene adipate-co-terephthalate) and miscanthus: preparation, compatibilization, and performance evaluation, J. Appl. Polym. Sci. 134 (43) (2017) 45448, https://doi.org/10.1002/app.45448.
[29] M.A. Abdelwahab, M. Misra, A.K. Mohanty, Injection molded biocomposites from polypropylene and lignin: effect of compatibilizers on interfacial adhesion and performance, Ind. Crop. Prod. 132 (2019) 497–510.
[30] F. Mai, C. Zhou, M. Yao, H. Deng, Q. Fu, Superior reinforcement in polyamide 1010/multiwalled carbon nanotube composites realized by high-rate drawing and incorporation of compatibilizer, Polym. Int. 61 (2012) 1400–1410.
[31] M. Hao, H. Wu, Z. Zhu, In situ reactive interfacial compatibilization of polylactide/sisal fiber biocomposites via melt-blending with an epoxy-functionalized terpolymer elastomer, RSC Adv. 7 (2017) 32399–32412.
[32] N.A. Nguyen, S.H. Barnes, C.C. Bowland, K.M. Meek, K.C. Littrell, J.K. Keum, A. K. Naskar, A path for lignin valorization via additive manufacturing of high-performance sustainable composites with enhanced 3D printability, Sci. Adv. 4 (2018), eaat4967, https://doi.org/10.1126/sciadv.aat4967. PMID: 30555914.
[33] R. Muthuraj, T. Mekonnen, Recent progress in carbon dioxide (CO2) as feedstock for sustainable materials development: Co-polymers and polymer blends, Polymer 145 (2018) 348–373, https://doi.org/10.1016/j.polymer.2018.04.078.
[34] R. Muthuraj, M. Misra, A.K. Mohanty, Biodegradable compatibilized polymer blends for packaging applications: a literature review, J. Appl. Polym. Sci. 135 (2018) 45726, https://doi.org/10.1002/app.45726.
[35] A. Duval, M. Lawoko, A review on lignin-based polymeric, micro- and nano-structured materials, React. Funct. Polym. 85 (2014) 78–96, https://doi.org/10.1016/j.reactfunctpolym.2014.09.017.
[36] T. Kikutani, Polymer Fibers: Formation and Structure,, in: K.H.J. Buschow, R. W. Cahn, M.C. Flemings, B. Ilschner, E.J. Kramer, S. Mahajan, T. Veyssière (Eds.), Encyclopedia of Materials: Science and Technology, Elsevier, Oxford, 2001, pp. 7288–7296, https://doi.org/10.1016/B0-08-043152-6/01298-5. ISBN 978-0-08-043152-9.
[37] F. Auriemma, V. Petraccone, L. Parravicini, P. Corradini, Mesomorphic form (β) of nylon 6, Macromolecules 30 (1997) 7554–7559.
[38] A. Anstey, A. Codou, M. Misra, A.K. Mohanty, Novel compatibilized nylon-based ternary blends with polypropylene and poly (lactic acid): fractionated crystallization phenomena and mechanical performance, ACS Omega 3 (2018) 2845–2854.
[39] T. Wu, M. Xiang, Y. Cao, J. Kang, F. Yang, Influence of lamellar structure on the stress–strain behavior of β nucleated polypropylene under tensile loading at elevated temperatures, RSC Adv. 5 (2015) 43496–43507.
[40] J.-R. Xu, X.-K. Ren, T. Yang, X.-Q. Jiang, W.-Y. Chang, S. Yang, A. Stroeks, E.-Q. Chen, Revisiting the thermal transition of β-form Polyamide-6: evolution of structure and morphology in uniaxially stretched films, Macromolecules 51 (2018) 137–150.
[41] B. Yin, L. Li, Y. Zhou, L. Gong, M. Yang, B. Xie, Largely improved impact toughness of PA6/EPDM-g-MA/HDPE ternary blends: the role of core–shell particles formed in melt processing on preventing micro-crack propagation, Polymer 54 (2013) 1938–1947.
[42] M. Culebras, A. Beaucamp, Y. Wang, M.M. Clauss, E. Frank, M.N. Collins, Biobased structurally compatible polymer blends based on lignin and thermoplastic elastomer polyurethane as carbon fiber precursors, ACS Sustain. Chem. Eng. 6 (2018) 8816–8825.
[43] A. Beaucamp, Y. Wang, M. Culebras, M.N. Collins, Carbon fibres from renewable resources: the role of the lignin molecular structure in its blendability with biobased poly(ethylene terephthalate), Green Chem. 21 (2019) 5063–5072, https://doi.org/10.1039/C9GC02041A.
[44] H. Kleinhans, L. Salmén, Development of lignin carbon fibers: evaluation of the carbonization process, J. Appl. Polym. Sci. 133 (2016) 43965, https://doi.org/10.1002/app.43965.
[45] L.M. Manocha, O.P. Bahl, G.C. Jain, Length changes in PAN fibres during their pyrolysis to carbon fibres, Die Angew. Makromol. Chemie Appl. Macromol. Chem. Phys. 67 (1978) 11–29.
[46] H.G. Chae, M.L. Minus, A. Rasheed, S. Kumar, Stabilization and carbonization of gel spun polyacrylonitrile/single wall carbon nanotube composite fibers, Polymer 48 (2007) 3781–3789.
[47] E.A. Morris, M.C. Weisenberger, M.G. Abdallah, F. Vautard, H. Grappe, S. Ozcan, F. L. Paulauskas, C. Eberle, D. Jackson, S.J. Mecham, High performance carbon fibers from very high molecular weight polyacrylonitrile precursors, Carbon N. Y. 101 (2016) 245–252.
[48] E.A. Morris, M.C. Weisenberger, S.B. Bradley, M.G. Abdallah, S.J. Mecham, P. Pisipati, J.E. McGrath, Synthesis, spinning, and properties of very high molecular weight poly (acrylonitrile-co-methyl acrylate) for high performance precursors for carbon fiber, Polymer 55 (2014) 6471–6482.